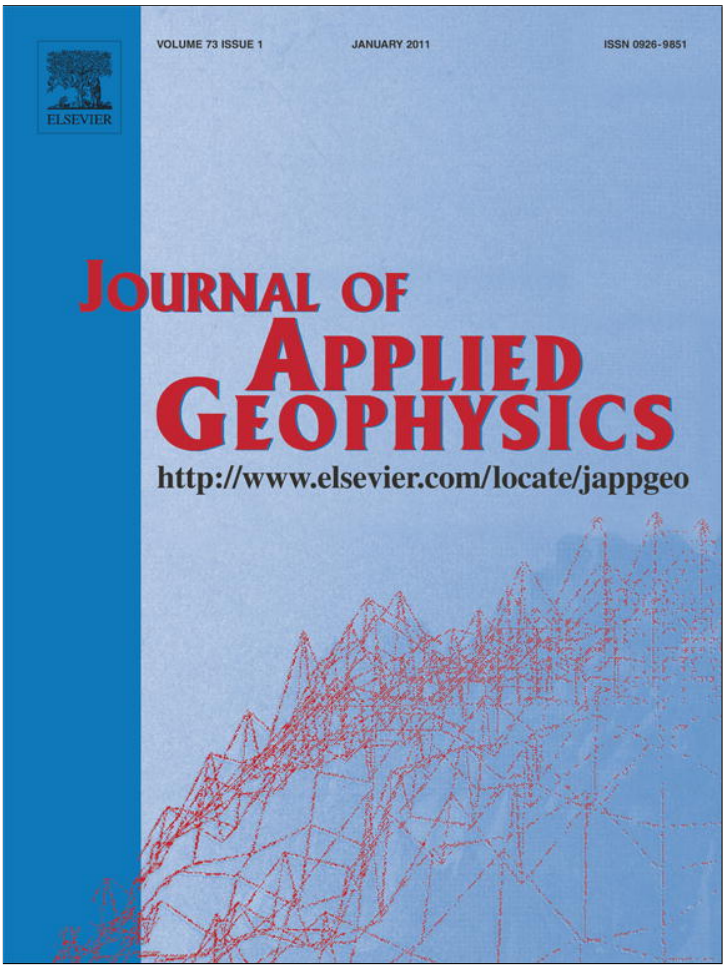

(This is a sample cover image for this issue. The actual cover is not yet available at this time.)

Journal of Applied Geophysics 77 (2012) 21–29

Contents lists available at SciVerse ScienceDirect

Journal of Applied Geophysics

journal homepage: www.elsevier.com/locate/jappgeo

Assessment of the distortions caused by a pipe and an excavation in the electric and electromagnetic responses of a hydrocarbon-contaminated soil

Hilda Patricia Martinelli [a,b,*], Fabiana Elizabeth Robledo [a,1], Ana María Osella [a,b], Matías de la Vega [a,b]

[a] Grupo de Geofísica Aplicada y Ambiental, Dto. de Física, Facultad de Ciencias Exactas y Naturales, Universidad de Buenos Aires. Ciudad Universitaria, Pabellón 1, Dto. de Fisica, 1428, Buenos Aires, Argentina
[b] IFIBA, CONICET, Argentina

ARTICLE INFO

Article history:
Received 27 January 2011
Accepted 22 October 2011
Available online 20 November 2011

Keywords:
Hydrocarbon contamination
Dual-coil, frequency domain, electromagnetic induction
Dipole–dipole geoelectric
3D numerical simulation
3D distortions caused by a pipe and an excavation

ABSTRACT

Here, we present the results of a geophysical survey performed to characterize a hydrocarbon contamination plume, arising from a puncture in a master crude oil pipe in Argentina. This pipe was buried in an inhabited suburban yard with flat topography. At the moment of the event a stretch of the duct was uncovered and the leaked oil flooded the terrain up to several meters around the puncture. The contamination was produced by infiltration from the surface and also by flowing through the inner layers. The first steps in the treatment of the spill were to pump the oil, excavate the sector nearby the puncture and repair the pipe. Around one year later, we preformed the geophysical prospecting, which goal was to determine the extent of the contaminant plume, required for selecting adequate remediation strategies. We combined dual-coil, frequency domain electromagnetic induction surveys and 2D dipole–dipole geoelectrical profiling. Besides, we performed Wenner soundings at several positions on the walls of the excavation, where contaminated and clean sediments were exposed. From the 1D inversion of the electromagnetic data, 2D inversion of the dipole–dipole data, and Wenner data, we found that, in general, the contamination decreased the resistivity of the affected subsoil volumes. However, three of the geoelectrical profiles exhibited localized, very resistive anomalies, which origin was not clear. They did not seem to be associated to the presence of high concentrations of poorly or non-degraded hydrocarbon, since two of these profiles crossed the more contaminated area, but the other was located quite further away. As an attempt to identify the cause of these anomalies, we carried out a 3D numerical simulation of the effects of the pipe and the excavation on the 2D dipole–dipole images. From this study, we could effectively determine that they were mainly distortions generated by those structures. This allowed for providing a proper interpretation of the images of the three profiles, consistent with the other results. Thus, we could finally delimit the impacted zone and ascertain the main features of the contaminant plume.

1. Introduction

Geophysical methods together with borehole geologic and geochemical data have been used during the last twenty years for the study of hydrocarbon contaminated sites (Atekwana and Atekwana, 2010). Also, these studies have been combined with hydrogeologic ones to see the possible influence of the contaminant plumes in the water resources.

In particular, geophysical techniques have been used to characterize hydrocarbon contaminant plumes, to determine their spatial extent and the properties of the substrate where they are contained, and to study if they have reach a water resource or could reach one in the future (Benson et al., 1997). Remediation strategies are designed taking into account this information, especially the latter (e.g. Coria et al., 2009). Geophysical techniques are also used as post-remediation devices to monitor the evolution and effectiveness of the applied remediation procedures (Halihan et al., 2005). These methods are widely used because through them it is possible to obtain 2D or 3D images of some physical property of the subsoil modified by the contaminant, at a comparatively low cost, in short time and in a non-invasive way. Relatively large areas can be covered to identify possibly contaminated sectors, some of which could not be detected by only using discrete coarse traditional methods. However, borehole data are important for adequately interpreting the geophysical results, since they provide the actual relation between the studied physical property of the soil – resistivity, dielectric constant, etc. – and the presence of contamination. Sometimes, due to the results of the geophysical analysis, it is necessary to drill new boreholes/wells in intermediate zones where the observed geophysical anomalies are at first difficult to interpret.

One of the principal problems of applying geophysical techniques for hydrocarbon contamination studies, in particular resistivity

* Corresponding author at: Grupo de Geofísica Aplicada y Ambiental, Dto. de Física, Facultad de Ciencias Exactas y Naturales, Universidad de Buenos Aires. Ciudad Universitaria, Pabellón 1, Dto. de Fisica, 1428, Buenos Aires, Argentina. Fax: +54 11 4576 3357.
E-mail address: pmartine@df.uba.ar (H.P. Martinelli).
[1] On a fellowship from Universidad de Buenos Aires.

0926-9851/$ – see front matter © 2011 Elsevier B.V. All rights reserved.
doi:10.1016/j.jappgeo.2011.10.016

techniques, is that the response of the soils to this kind of contamination has a very complex nature and is time varying (Atekwana and Atekwana, 2010). Besides, complete 3D geophysical studies if not correctly designed could take too much time and not be economically viable. The latter problem could be resolved by performing high resolution 2D profiles, together with less resolution 3D surveys, which combined with borehole data can permit a correct characterization of the contaminated zone.

As just stated, the complexity of resistive studies of hydrocarbon spills is mainly due to the time changing nature of resistivity in this type of spills. Hydrocarbons are highly resistive; then, immediately after the leakage, as hydrocarbon replaces conductive water in pore spaces the spill presents a highly resistive nature (Lien and Enfield, 1998). This may change in time. In fact, aged spills (above 30 years old) present low resistivity values (Werkema et al., 2003). After some months (4 to 12, Shevnin et al., 2005) a hydrocarbon spill may totally or partially present low electrical resistivity. This is due to superficial conductivity increase in soil pores induced by hydrocarbon biodegradation products (Abdel Aal et al., 2004). This process depends on different factors such as sand/clay relation in soil composition, pore microstructure and volume, etc. (Shevnin et al., 2006). It not always takes place, or can take place very weakly. For example, a study performed by our group (de la Vega et al., 2003) of a four year old hydrocarbon leakage showed high resistivity values.

In this work, we present the results obtained in the study of a leakage of crude oil due to a puncture of a master oil duct. The leakage occurred in an inhabited suburban yard, of approximately 100 m by 100 m, with flat topography. The involved pipe, a 1 m-diameter metallic tube with an isolating resistive covering, is buried at approximately 1.5 m deep. At the moment of the event a stretch of the pipe was uncovered and the leaked oil flooded the terrain up to several meters around the puncture. The contaminant was soon pumped and after that, the sector nearby the puncture was excavated and the pipe was repaired. The affected soil was contaminated due to infiltration from the surface and also from flowing through the inner layers. There was also a considerable risk that the contamination could have reached the water table. We preformed the geophysical prospection about one year after the event. The goal of the study was to determine the extension of the contaminant plume, required for selecting adequate remediation strategies.

The geophysical methods used were dual-coil, frequency domain electromagnetic induction surveys, performed with a GEM-2 system (Geophex Ltd.), and 2D dipole–dipole geoelectric profiling using a SARIS 500 equipment (Scintrex). With both methods the resistivity of the subsoil is studied. We performed 1D inversions of the GEM-2 data (Farquharson et al., 2003) and, from these results, obtained pseudo-3D electrical images of the subsoil. The dipole–dipole data were inverted using the 2D method DCIP2D (Oldenburg and Li, 1994; Oldenburg et al., 1993). Combining these results, a good representation of the subsoil resistivity was obtained in general, though the interpretation of some of the observed anomalies was not clear. Considering this, we performed a numerical simulation study of the effects of the duct and the excavation on the geoelectrical images, in order to determine if these effects could explain the origin of those anomalies. We proposed a schematic 3D model representative of the structures present in the studied site, including the pipe and the excavation. The subsoil model was selected considering information obtained from GEM-2 data and borehole data, at long distance away from the duct. Using the code DCIP3D (Li and Oldenburg, 1994), we calculated the synthetic dipole–dipole geoelectric responses of this 3D model, for lines parallel and perpendicular to the pipe, and then we inverted these responses using the code DCIP2D. Finally, we performed a global interpretation of the results, considering the effects produced by the presence of the duct and the excavation, which allowed for obtaining an adequate characterization of the contaminant plume.

2. Site description

The incident occurred at an unoccupied field of a suburban site, with quite flat topography. The involved pipe corresponds to a master crude oil pipeline system; it consisted of a 1 m-diameter metallic tube, with an isolating resistive covering, buried at approximately 1.5 m deep. At the moment of the event a stretch of the pipe was uncovered and the leaked oil flooded the terrain up to several meters around the puncture, mainly in the NE–SW direction. The contaminant was soon pumped. After that, the sector nearby the puncture was excavated, the soil was removed for remediation and the pipe was repaired (Fig. 1a). The effects of the spill can be clearly seen in this excavation (Fig. 1a and b). In the affected area, the soil was contaminated not only due to infiltration from the surface but also from flowing through the inner layers. There was also a considerable risk that this infiltration could reach the phreatic layer, which was about 3–4 m deep, with a hydraulic NW slow slope. The area was limited to the NW by a dense wood that ended some meters further at a riverside. Within this context, we planned the prospection in order to determine the extension of the contaminant plume, needed for selecting the remediation strategies. The study was performed approximately one year after the event.

As previous data, we had analysis from two wells inside the field, located 8 m and 35 m SE of the pipe, respectively (see Fig. 1c). Neither of them revealed contaminated groundwater. The stratigraphy of the site up to a depth of 10 m was also known from these wells. First, there was a 2 m thick layer of silt loam, below this, a 2 m thick layer of silty clay, then a 4 m thick layer of sandy loam and finally clay.

3. Data acquisition and processing

We combined the geoelectrical and electromagnetic induction methods. We first conducted an electromagnetic survey using a dual-coil, multi-frequency, electromagnetic induction system GEM-2 (Geophex). This system consists of two coplanar small coils, a transmitter (Tx) and a receiver (Rx), separated by a constant distance, which are moved along profiles, at a nearly constant height. The secondary magnetic field detected at the receiver is decomposed into in-phase (HI) and quadrature (HQ) components, which are expressed in PPM (parts per million) of the primary field. As shown in Fig. 1c, we covered two sectors: GEM-S1 and GEM-S2. Data were acquired along parallel lines, spaced 0.5 m, in two perpendicular directions, coincident with the ones of the x- and y-axes, respectively. We also performed two lines in the SE and SW directions, GEM-L1 and GEM-L2, respectively. As our target depths were expected to be 5–6 m, we selected the following six frequencies: 2575, 3925, 8775, 13,575, 30,375 and 47,025 Hz.

We first applied to the data smoothness constrains to remove outliers that distort the inversion procedure and then used a lateral filtering technique for improving the signal-to-noise ratio (Martinelli and Duplaá, 2008; Martinelli and Osella, 2010). Next, these data were inverted using the 1D inversion code EM1D v1.0, developed at the University of British Columbia (UBC) by Farquharson et al. (2003), to obtain a model of the electrical conductivity distribution below each measurement point. Finally, these models were stitched-together to build up pseudo-2D and 3D electrical images for the prospected lines and sectors, respectively.

The geoelectrical surveys were performed employing a Saris 500 equipment (Scintrex). We acquired five dipole–dipole lines, with apertures $a = 1.5$ and 3 m, and maximum values of $n = 8$ and 6, respectively (Fig. 1c). To obtain the electrical images, these data were inverted using the DCIP2D inversion code developed at the UBC by Oldenburg et al. (1993) and Oldenburg and Li (1994). Data acquired with apertures $a = 1.5$ and 3 m were inverted together to improve the resolution of the models.

Taking advantage of the exposed contaminated layers, we also performed five Wenner soundings on the walls of the excavation, at depths around 0.7–0.9 m, with electrode separations 0.25, 0.35 and

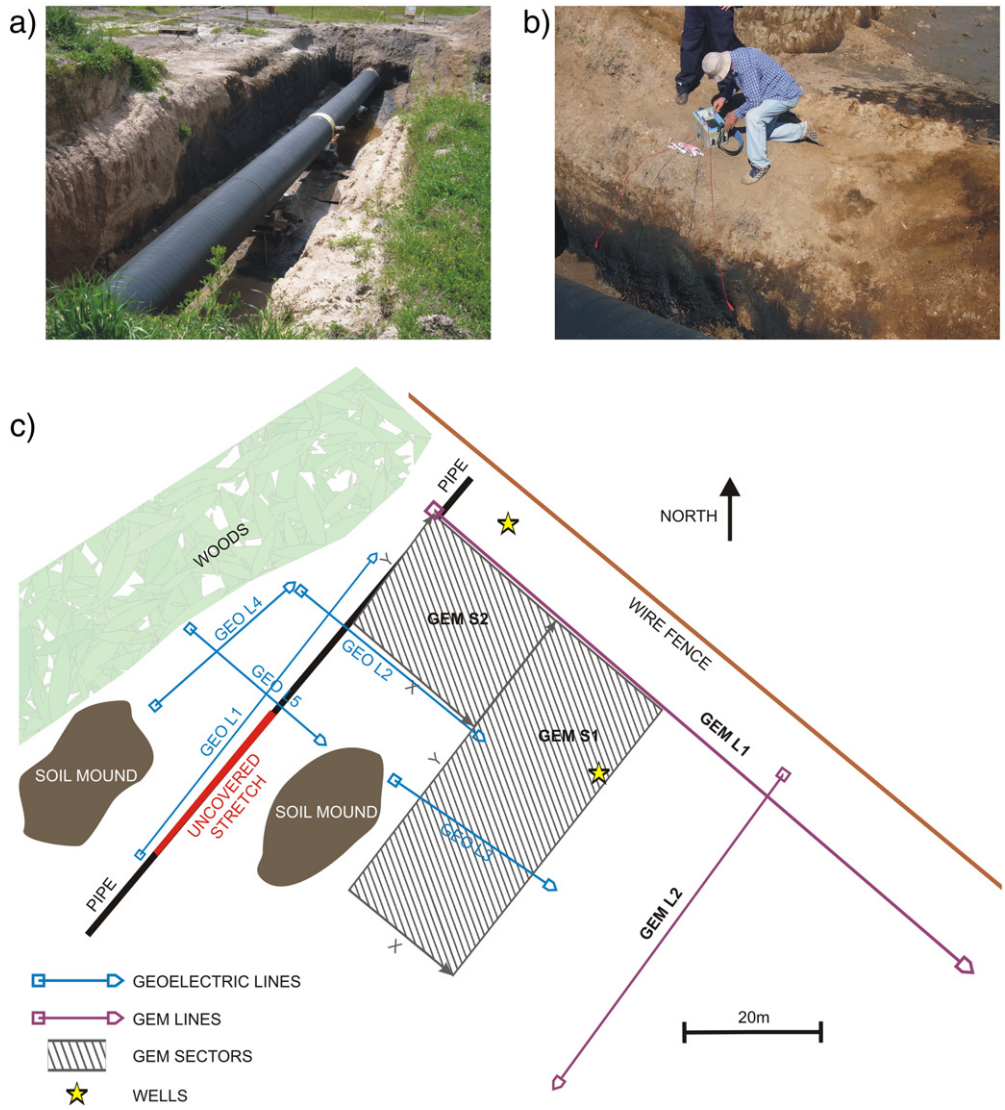

Fig. 1. a) Exposed pipe after the spill. Contaminated soil is shown. b) Detailed photo showing the impact of the spill, at a wall of the excavation where one of the Wenner soundings was deployed. c) Map of the site. The location of the GEM and dipole–dipole geoelectrical surveys is indicated, as well as the position of two wells.

0.45 m (Fig. 1b). Three of them were located on contaminated layers and two on sectors that had not been impacted. The goal of these measurements was to get an estimation of the relative signature of the contaminant in the subsoil that aid to interpret the electrical images obtained from the inversion of the dipole–dipole data.

4. Results from the GEM-2 surveys

4.1. Lines GEM-L1 and GEM-L2

We first analyzed lines GEM-L1 and GEM-L2, which were located close to the wells (Fig. 1c). Except for the zone of line GEM-L1 closest to the metallic pipe, the electrical images obtained from the 1D inversion of these data are similar for both lines, and exhibit a layered structure without significant lateral anomalies. As an example, we show the model obtained along part of the line GEM-L1 (Fig. 2). This model is consistent with the information obtained from the wells. The second resistive layer corresponds to the phreatic zone, which begins at the expected depth of about 4 m and lies on top of the highly conductive and poorly permeable clay layer. Between 2 and 4 m deep, approximately, there is another conductive layer, which corresponds to the silty clay, and above it there are more resistive, near surface sediments. The lateral uniformity along both profiles indicates the absence of detectable contamination disturbing the soil.

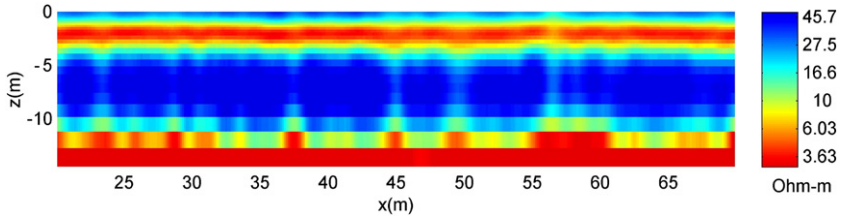

Fig. 2. Electrical image obtained from the 1D inversion of data corresponding to the line GEM-L1 (see Fig. 1c).

4.2. Sector GEM-S1

This sector has an area of 20 m × 50 m and was located approximately 20 m away from de pipe; at this distance, the effect of the pipe on data can be neglected. It is interesting to analyze this sector since the surface between x = 0–7 m and y = 0–35 m, was covered after the accident by a flow of hydrocarbon. Fig. 3 shows the 3D electrical image built up from the 1D inversion of data. The analysis of this image can be done by comparison to the ones obtained for the GEM-L1 and L2 profiles. A first result in regards to the impact of the flood is that it produced a decrease of the electrical resistivity in the first layer, as can be observed in Fig. 3a and b. As going deeper, we see that the phreatic layer also became more conductive due to the presence of the contaminant (Fig. 3e and f). For values of x lower than about 10 m, the contamination seems to spread almost along the whole y direction, though the most contaminated zone corresponds, approximately, to the area 0<x<8 m, 20<y<34 m, as can be clearly appreciated from Fig. 4. Towards the borders of the Sector in the x and y directions, the model tends to recover the behaviour shown at GEM-L2.

4.3. Sector GEM-S2

This sector has an area of 25 m × 20 m; the y-axis was located close to the pipe, so the first meters on the x-direction are affected by its presence (Fig. 1c). The corresponding electrical image is shown in Fig. 5. In this case, the conductive anomaly produced by the metallic pipe is superimposed to the anomalies originated by the contaminant. Despite this, the most contaminated area still can be delineated and corresponds to values of x and y between 0 and 10 m, approximately. For x greater than about 10 m, the response recovers the behaviour observed at GEM-L1. Again, the contamination decreased the resistivity in the upper layer and reached the groundwater; although at the time of the study, the plume had not appreciably migrated and still remained confined to the aforementioned region, probably due to the quite low hydraulic slope and the moderate time elapsed between the spill and the electromagnetic survey.

5. Results from the geoelectric surveys

5.1. Wenner soundings

As previously explained, we performed Wenner soundings at the vertical walls of the excavation, three located on contaminated zones and two at non-impacted ones. In each case, we employed only three different electrode-apertures, taking into account that our goal was just to determine the signature of the anomaly produced by the contaminant in the electrical resistivity of the upper layer of sediments (the one located over the silty clay layer). It is clear that as these sediments were exposed, their conditions of humidity and temperature were modified respect to the ones in the corresponding buried layer, but the signature of the anomaly produced by the

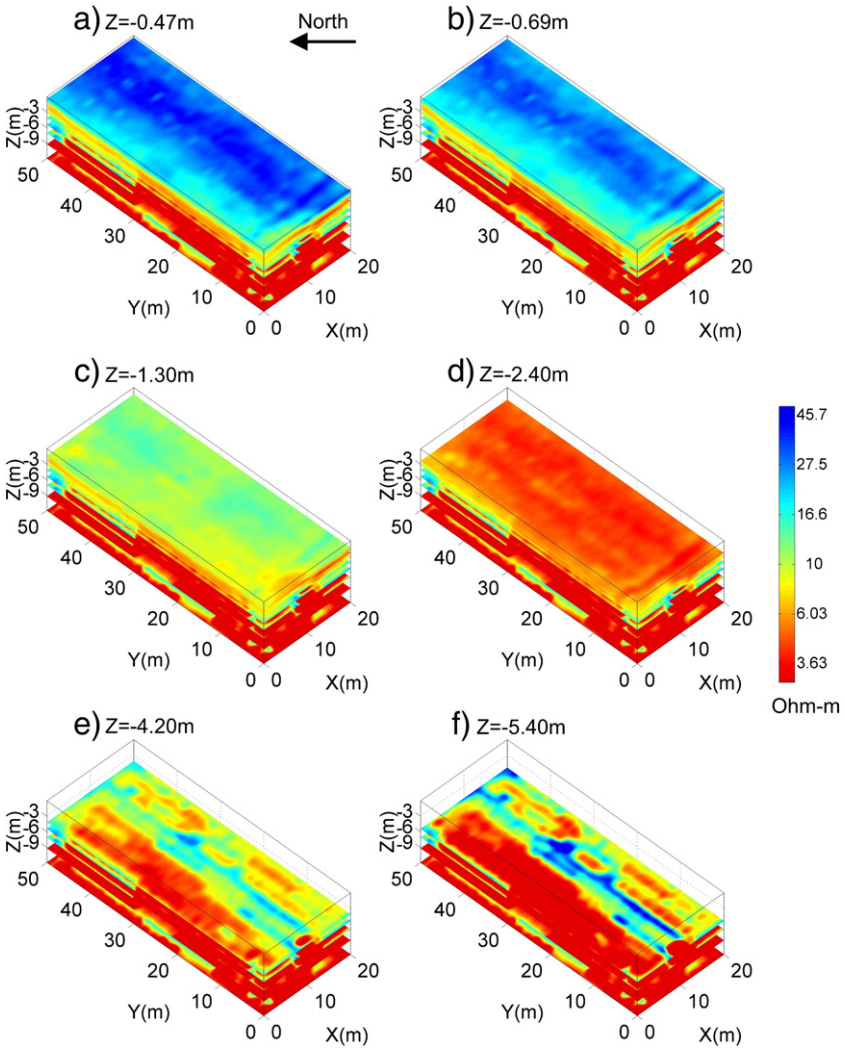

Fig. 3. The same as in Fig. 2, for the sector GEM-S1 (see Fig. 1c).

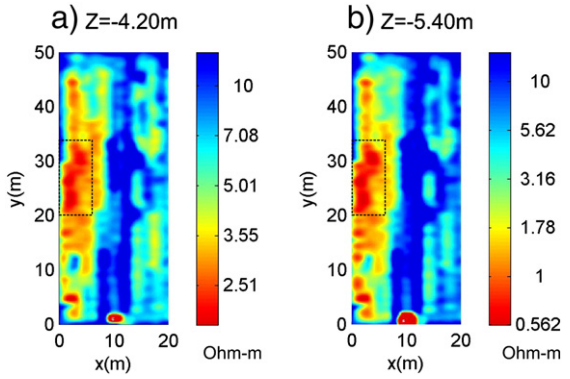

Fig. 4. a) and b) More detailed views of the slices shown in Fig. 3e and f, respectively. The most contaminated area has been marked.

hydrocarbon should remain unchanged, since both the contaminated and the clean sediments were both equally exposed to weathering effects.

The average apparent resistivity value for the Wenner soundings carried out at the contaminated areas, was 17.8 Ω-m, with standard deviation 1.6 Ω-m. At the clean zones, the average apparent resistivity was higher, 35.2 Ω-m, with standard deviation 2.8 Ω-m . This indicates that the contaminant reduced the resistivity of the soil, which is in agreement with the conclusion obtained from the interpretation of the GEM-S1 and GEM-S2 data.

5.2. Dipole–dipole profiles

The location of these profiles is shown in Fig. 1c. The electrical images obtained from the 2D inversion of data from the profiles parallel to the pipe (GEO-L1 and GEO-L4) and perpendicular to it (GEO-L2, GEO-L3 and GEO-L5) are shown in Figs. 6 and 7, respectively.

Line GEO-L1 was parallel to the pipe and the closest to it. For x greater than about 32 m, an increase of the resistivity is again observed near the expected depth of the phreatic layer; the conductive layer located above the phreatic is also clearly detected. In general, there are lateral resistivity anomalies throughout the whole profile, and the shallower layer has lower resistivity than in the other sectors, with some interruptions. Towards the end of the profile, for $x > 45$ m, the results are consistent with those observed in the sector GEM-S2 (Fig. 5) for the shallower layers, although overall resistivities were lower than in that GEM sector, due to the conductive anomaly associated to the inductive currents generated on the metallic pipe despite of its isolation. Near the excavated zone, the conductivities detected about the depths of the silty clay layer are lower than for $x > 32$ m. A conductive anomaly is detected close to the puncture, with its top near $z = -4$ m. On the contrary, a highly resistive anomaly is observed for $x < 12$ m and $z < -3.5$, approximately.

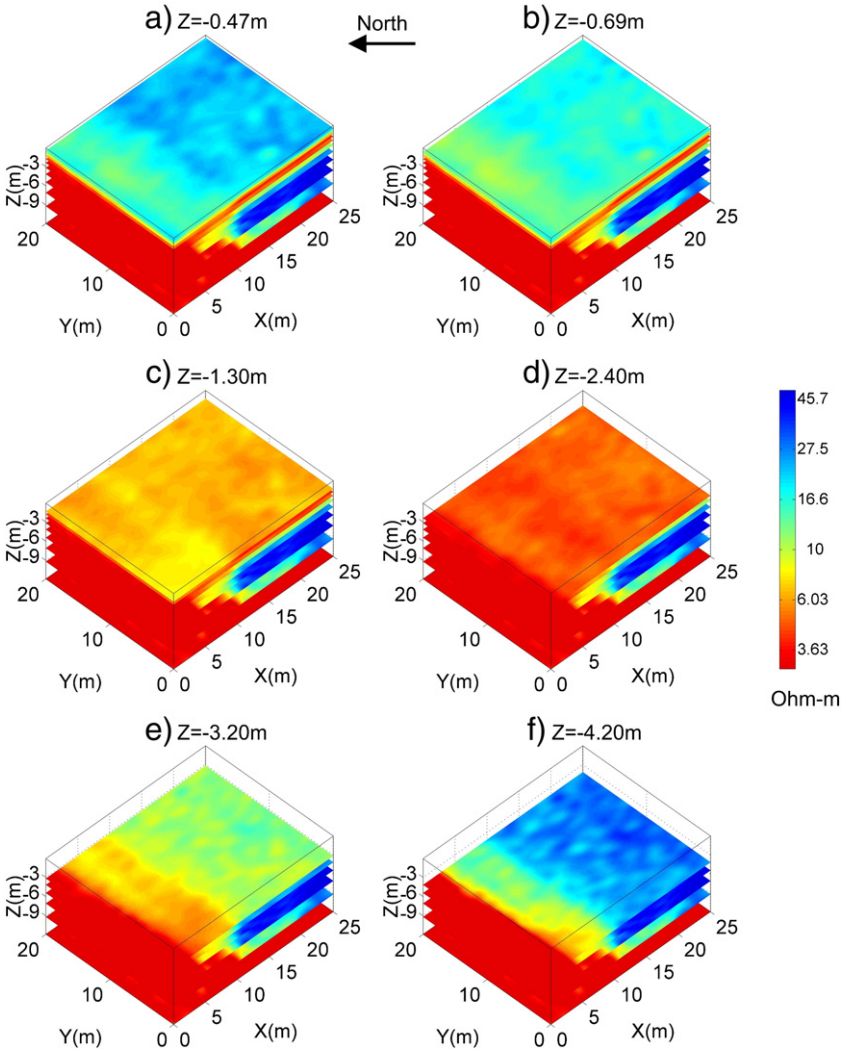

Fig. 5. The same as in Fig. 2, for the sector GEM-S2.

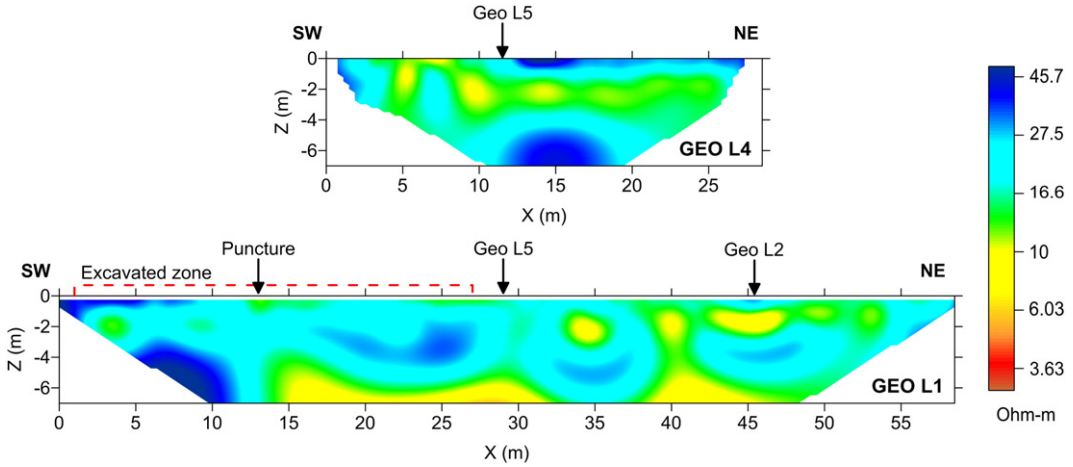

Fig. 6. Electrical images obtained from the 2D inversion of the dipole–dipole geoelectrical data acquired at the profiles parallel to the pipe (see Fig. 1c).

Line GEO-L4 was deployed close to the border of the wood, around 7 m NW from GEO-L1. For $x > 12$ m, the shallower layer is more resistive than in the previous case; again, there is a conductive layer below it that is somewhat deeper than at GEO-L1. Resistivity increases as going downwards. One interesting feature is that a highly resistive anomaly is again present between $x = 12$ and 18 m, for $z < -5$ m, approximately. This anomaly is similar to the one encountered at GEO-L1, for $x < 12$ m, although it is located deeper. For $x < 12$ m, there are more lateral inhomogeneities.

The perpendicular profiles (Fig. 7) present some distinctive features. Lines GEO-L2 and GEO-L5 crossed the pipe at the indicated positions. Due to the isolating covering and the cathodic protection, the injected currents practically did not flow towards the pipe, which was therefore detected by this method as a resistive object.

In GEO-L2, from $x = 8$ to 13 m, approximately, the upper conductive layer is interrupted by the effect of the pipe. Besides, an important conductive anomaly is detected for $z < -4$ m, extending from $x = 5$ to about 20–22 m, and centered almost under the pipe. For greater x values, the electrical structure tends to recover the behaviour corresponding to uncontaminated soil. These results are in agreement with the ones obtained for the sector GEM-S2 (Fig. 5).

GEO-L5 was closer to the puncture and the excavation than GEO-L2. Again, the more conductive layer is interrupted due to the presence of the pipe. The difference with GEO-L2 is that the conductivity below the pipe is much lower. Furthermore, a highly resistive anomaly is detected at about 4.5 m depth, spreading between $x = 8$ m and $x = 15$ m, approximately, analogous to the ones observed at the profiles GEO-L1 and GEO-L4.

The line GEO-L3 is the continuation of GEO-L5 and intersects the sector GEM-S1 (see Fig. 1c). The results obtained for this line are in coincidence with the image obtained for that sector (Figs. 3 and 4). A clear conductive anomaly is detected from a depth of about 4 m, for $x < 17$ m, approximately, similar to the one present at GEO-L2. The interesting result is that both conductive anomalies are aligned in the NW direction, which coincides with the hydraulic flow slope.

Considered as a whole, the obtained results seem to present some contradictions. We dealt with a hydrocarbon spill about one year old. The electrical images obtained from the inversion of GEM-2 data for sectors GEM-S1 and GEM-S2, together with the results of the Wenner soundings at exposed layers, suggest that the contaminated zones exhibit a general increase of the electrical conductivity that includes the phreatic layer. Other than that, localized, highly resistive anomalies are observed in depth at GEO-L1 and GEO-L5, which cross the region where more contamination was expected. However, their main cause does not seem to be an accumulation of poorly or non-degraded hydrocarbon in the phreatic layer, since the same type of resistive anomaly is present in depth at GEO-L4, which is considerably further from the puncture. Considering this, we decided to perform numerical simulations to evaluate the effects of the pipe and the excavation on the geoelectrical images, and figure out if these effects could provide a plausible explanation of the origin of these and other resistive anomalies observed in the geoelectrical models.

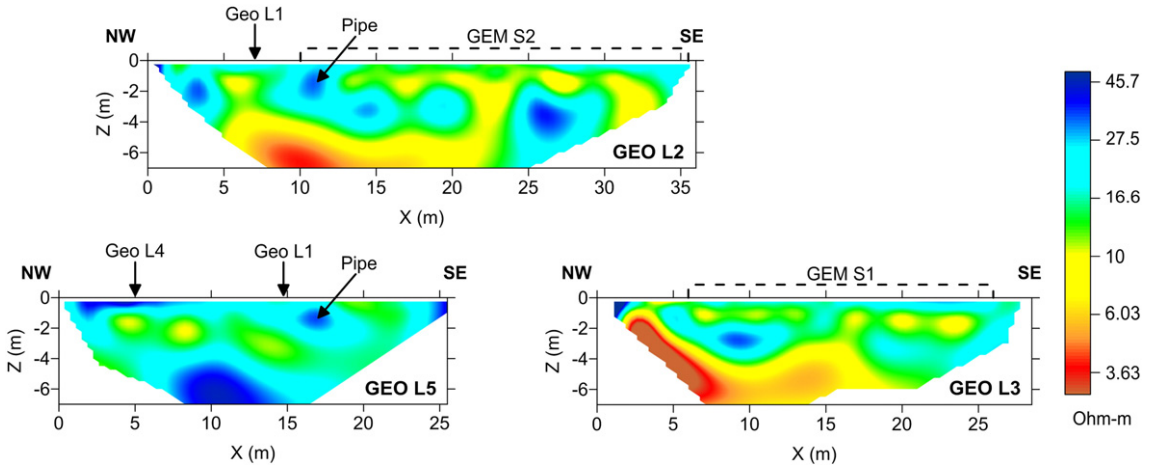

Fig. 7. The same as in Fig. 6, for the profiles perpendicular to the pipe.

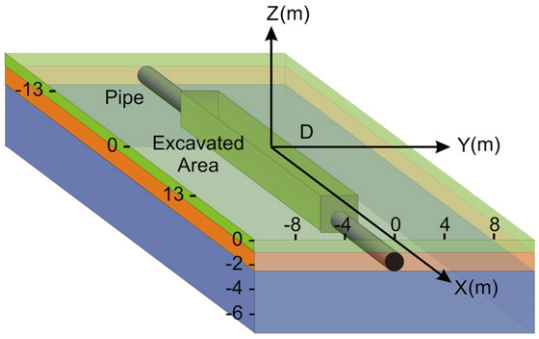

Fig. 8. Schematic model used for the numerical simulations, which is representative of the main structures present at the studied site, including the pipe and the excavation. Since, due to the isolating covering and the cathodic protection, the injected currents almost do not flow into the pipe, it is considered as a resistive object.

6. 3D effects of the pipe and the excavation on the 2D geoelectrical images

The geoelectrical images were obtained from the 2D inversion of the dipole–dipole profiles. Nevertheless, the actual structure is not 2D; both the pipe and the excavation produce 3D effects that can not be properly determined through a 2D analysis, especially for lines parallel to the pipe, and so can lead to mistakes in the interpretation.

To have a qualitative estimation of these effects, we performed numerical simulations using 2D and 3D codes. We considered the schematic 3D model shown in Fig. 8, in which a pipe is embedded in a three layer subsoil. The parameters selected for the pipe and the background are representative of the structures encountered at the studied site (from Fig. 2). The subsoil consists of an upper layer with thickness 1.5 m and resistivity 30 Ω-m, a second conductive layer with thickness 1 m and resistivity 8 Ω-m, and a half-space with resistivity 60 Ω-m. The pipe has a diameter 1 m and is buried between the depths 1.5 and 2.5 m. We also included an excavation like that present at the site, 27 m long, 3 m wide and 3 m deep, which is represented as a medium of resistivity 1000 Ω-m. According to the previous discussion, the pipe is also considered as a resistive object, with resistivity 200 Ω-m. We simulated the 3D response of this model using the DCIP3D code (Li and Oldenburg, 1994), obtaining synthetic dipole–dipole geoelectric data for lines parallel and perpendicular to the pipe. For the central region of the model, we used a mesh made up of 312×108×24 cells, each one with dimensions 0.25 m×0.2 m×0.25 m. So, the size of this region was 78 m×27 m×6 m, in the x, y and z directions, respectively. This mesh was extended beyond that region with cells of increasing dimensions, covering an entire volume of 105 m×54 m×15 m. The total number of cells used was 2,150,148. We added to the calculated synthetic responses Gaussian random noise of standard deviation 5% and then, inverted them using the DCIP2D code. In this way we could evaluate the influence of the pipe and the excavated zone, basically 3D effects, when inverting the data using 2D methods.

The models obtained for profiles parallel to the pipe are shown in Fig. 9. We can see an increase in the resistivity due to the excavation, which deepens as going away from this structure, and becomes negligible for $y > 10.5$ m. The lateral extension of this resistive anomaly is similar to that of the excavation, approximately 25 m. On the other side, the effect of the pipe, located within the conductive layer, is detected only at the closer profiles, $y < 3$ m, as a decrease in the conductivity of the conductive layer.

The images obtained for the perpendicular profiles are shown in Fig. 10. The profile at $x = 13.5$ m, located close to the border of the excavation, clearly shows its effect superposed to the influence of the pipe, as an interruption in the conductive layer. Moving further, at $x = 15$ m, the effect of the pipe remains as a decrease of the conductivity of the conductive layer where the pipe is located, and the excavation produces a deeper, resistive anomaly. For $x = 16.5$ m, the pipe has the same effect while the resistive anomaly associated to the excavation becomes even deeper. For $x > 18$ m the influence of the excavation is barely detectable.

7. Interpretation of the geoelectrical results considering the 3D effects

With these results in mind, we can now complete the interpretation of the dipole–dipole profiles. GEO-L1 and GEO-L4 (Fig. 6) are profiles parallel to the pipe, approximately located 2 m and 7 m away from it. Comparing the images at these profiles with the models shown in Fig. 9, we can identify the deep resistive anomaly observed at both profiles mainly as a 3D distortion effect due to the excavation. This anomaly appears at a depth of about 3.5 m in GEO-L1 ($x < 12$ m),

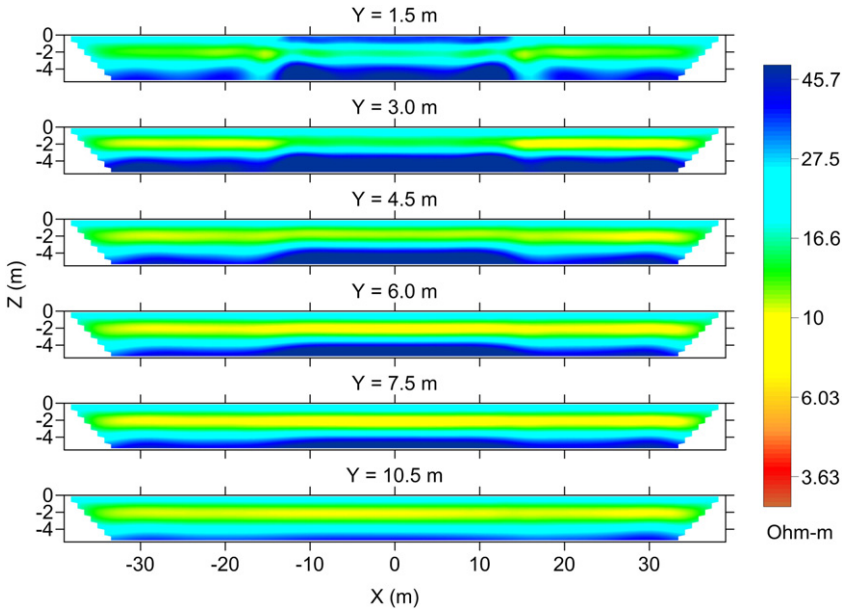

Fig. 9. Electrical images parallel to the pipe, obtained from the 2D inversion of the synthetic 3D geoelectical responses calculated for the model shown in Fig. 8.

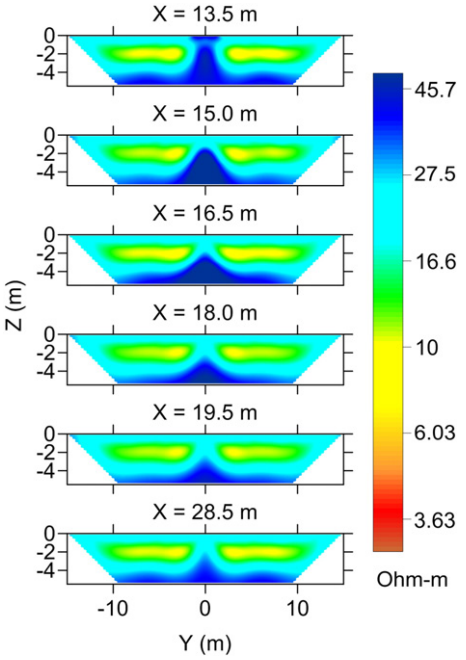

Fig. 10. Electrical images perpendicular to the pipe, obtained like the ones shown in Fig. 9.

and at a depth of 5 m at GEO-L4, which is in good agreement with the results from the numerical simulations, in spite of the approximations in the proposed schematic model. The decrease in the conductivity of the upper conductive layer observed at GEO-L1 along the excavation also seems to be mostly a 3D effect produced by this structure.

Regarding the perpendicular profiles (Fig. 7), GEO-L5 is located close to the border of the excavation ($x = 15$ m) and GEO-L2 is further, approximately at $x = 30$ m. Comparing with the results shown in Fig. 10, the deep resistive anomaly found in GEO-L5 once again can be associated with a 3D effect of the excavation, while the breaking of the upper conductive layer seems to be caused by the pipe. This last effect is also detected at GEO-L2. Besides, as this profile is far from the excavation, no deep resistive anomaly is observed. GEO-L3 is not affected either by the pipe or the excavation.

To complete the analysis, we calculated the effects produced by the pipe and the excavation, but considering the pipe as conductive. The geometry of both structures is the same as before, except that the resistivity of the pipe is now 2 Ω-m and the background is a uniform half-space with resistivity 40 Ω-m. The results for the parallel and perpendicular profiles are shown in Figs. 11 and 12, respectively. The effects of the pipe and the excavation on the responses are different from those observed in our study, mainly for the perpendicular profiles. This confirms that the covering of the pipe electrically isolates it from the soil, and so it must be considered resistive for the geoelectrical method.

8. Conclusions

In this work, we present the results of a geophysical study of a hydrocarbon spill. This study was preformed about one year after the event, and its goal was to determine the extent of the contaminant plume.

First, using a multifrequency, dual-coil induction system, GEM-2, we measured two profiles located outside the impacted area, in order to have a reference for the structure of the uncontaminated soil. The electrical images obtained indicated a laterally uniform soil, with the water-table located at approximately 3-4 m deep. Then, we covered with this method two areas close to the spill, and the results suggested that the effect of the contaminant was a decrease in the resistivity of both the shallower and the phreatic layers. For the shallower layer, this result was confirmed by Wenner surveys done on the vertical walls of the excavation, where both impacted and clean sediments were exposed.

To complete the analysis and constrain the location of the contaminant plume, we deployed five dipole–dipole geoelectrical profiles. From those images and in agreement with the GEM-2 and Wenner results, we found a general decrease of the resistivity of the upper layer at contaminated zones. Also, a large conductive anomaly was detected in depth at two of the profiles. It had a NW direction, coincident with that of the hydraulic flow. The other three profiles contained in depth, localized, highly resistive anomalies, which main cause was at first difficult to determine. They did not seem to be attributable to accumulations of poorly or non-degraded hydrocarbon in the phreatic layer, since they were present not only at the two

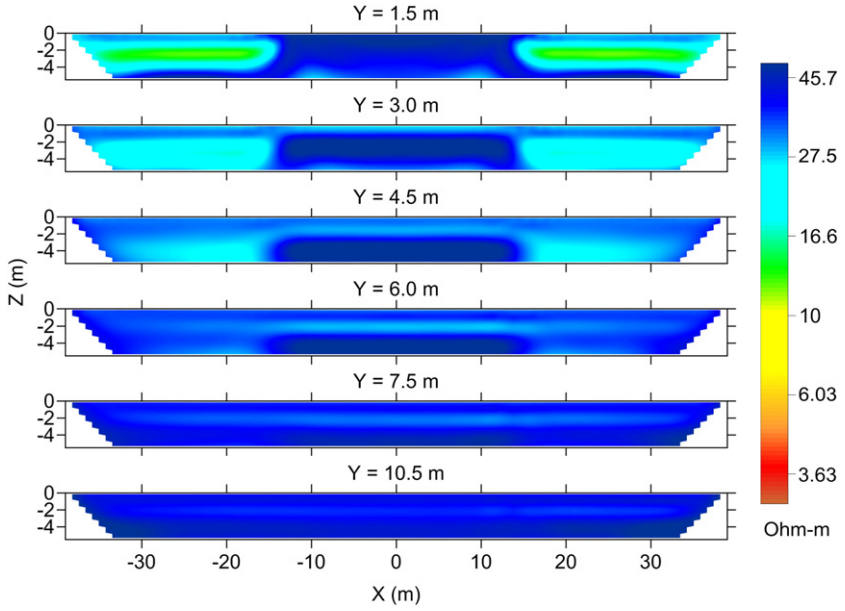

Fig. 11. Electrical images parallel to the pipe, obtained from the 2D inversion of the synthetic 3D geoelectrical responses of a model similar to that shown in Fig. 8, except that now the pipe is conductive (2 Ω-m), and is embedded in a uniform half-space of resistivity 40 Ω-m.

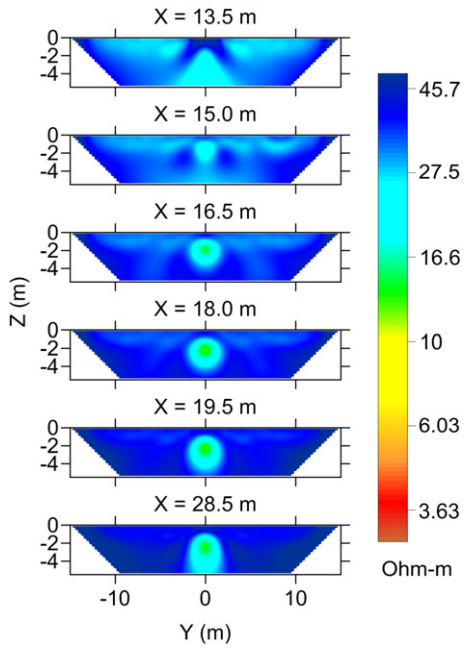

Fig. 12. Electrical images perpendicular to the pipe, obtained like the ones shown in Fig. 11.

profiles that crossed the more contaminated area, but also at the profile that was located considerably further. Through a numerical simulation study, carried out combining 3D forward and 2D inverse geoelectrical modelling, we could establish that the most probable origin of these anomalies were the distortions of the 2D geoelectrical images produced by the presence of the duct and the excavation. This conclusion was important for appropriately interpreting the images of these three profiles, and assured that they did not contradict the GEM-2 results.

Considering the described results as a whole, we could delimit the impacted zone and ascertain the main features of the contaminant plume.

Acknowledgments

This work was partially supported by Conicet and ANPCyT.

References

Abdel Aal, G., Atekwana, E.A., Slater, L.D., 2004. Effects of microbial processes on electrolytic and interfacial electrical properties of unconsolidated sediments. Geophysical Research Letters 31, L12505.

Atekwana, E.A., Atekwana, E.A., 2010. Geophysical signatures of microbial activity at hydrocarbon contaminated sites: a review. Surveys in Geophysics 31, 247–283.

Benson, A.K., Payne, K.L., Stubben, M., 1997. Mapping groundwater contamination using dc resistivity and VLF geophysical methods – a case study. Geophysics 62 (1), 80–86.

Coria, D., Bongiovanni, M.V., Bonomo, N., de la Vega, M., Garea, M.T., 2009. Hydrocarbon contaminated soil: geophysical–chemical methods for designing remediation strategies. Near Surface Geophysics 7 (3), 227–236.

de la Vega, M., Osella, A., Lascano, E., 2003. Joint inversion of Wenner and dipole–dipole data to study a gasoline-contaminated soil. Journal of Applied Geophysics 54, 97–109.

Farquharson, C.G., Oldenburg, D.W., Routh, P.S., 2003. Simultaneous 1D inversion of loop-loop electromagnetic data for magnetic susceptibility and electrical conductivity. Geophysics 68 (6), 1857–1869.

Halihan, T., Paxton, S., Graham, I., Fenstemaker, T., Riley, M., 2005. Post-remediation evaluation of a LNAPL site using electrical resistivity imaging. Journal of Environmental Monitoring 7, 283–287.

Li, Y., Oldenburg, D.W., 1994. Inversion of 3-D DC resistivity data using an approximate inverse mapping. Geophysical Journal International 116 (3), 527–537.

Lien, B.K., Enfield, C.G., 1998. Delineation of subsurface hydrocarbon contaminated distribution using a direct push resistivity method. Journal of Environmental and Engineering Geophysics 2–3, 173–179.

Martinelli, H.P., Duplaá, M.C., 2008. Laterally filtered 1D inversions of small-loop, frequency-domain EMI data from a chemical waste site. Geophysics 73 (4), F143–F149.

Martinelli, H.P., Osella, A.M., 2010. Small-loop electromagnetic induction for environmental studies at industrial plants. Journal of Geophysics and Engineering 7, 91–104.

Oldenburg, D.W., Li, Y., 1994. Inversion of induced polarization data. Geophysics 59, 1327–1341.

Oldenburg, D.W., McGillivary, P.R., Ellis, R.G., 1993. Generalized subspace method for large scale inverse problems. Geophysical Journal International 114, 12–20.

Shevnin, V., Delgado-Rodríguez, O., Fernández-Linares, L., Zegarra Martínez, H., Mousatov, A., Ryjov, A., 2005. Geoelectrical characterization of an oil-contaminated site in Tabasco, Mexico. Geofísica Internacional 44 (3), 251–263.

Shevnin, V., Delgado-Rodríguez, O., Mousatov, A., Flores Hernández, D., Zegarra Martínez, H., Ryjov, A., 2006. Estimation of soil petrophysical parameters from resistivity data: application to oil-contaminated site characterization. Geofísica Internacional 45 (3), 179–193.

Werkema Jr., D.D., Atekwana, E.A., Endres, A.L., Sauck, W.A., Cassidy, D.P., 2003. Investigating the geoelectrical response of hydrocarbon contamination undergoing biodegradation. Geophysical Research Letters 30, 1647.